coatings

MDPI

Article

Comparison of Friction Behaviour of Titanium Grade 2 after Non-Contact Boriding in Oxygen-Containing Medium with Gas Nitriding

Serhii Lavrys [1,*], Iryna Pohrelyuk [1], Oleh Tkachuk [1], Juozas Padgurskas [2], Vasyl Trush [1] and Roman Proskurnyak [1]

[1] Department of Material Science Bases of Surface Engineering, Karpenko Physico-Mechanical Institute of the NAS of Ukraine, 79060 Lviv, Ukraine
[2] Department of Mechanical, Energy and Biotechnology Engineering, Vytautas Magnus University, 44248 Kaunas, Lithuania
* Correspondence: lavrys92@gmail.com; Tel.: +38-0938421426

Abstract: The surface characteristics and friction behaviour of titanium Grade 2 with modified nitride (TiN, Ti_2N) and boride (TiB) compound layers were investigated. It was shown that during non-contact boriding in oxygen-containing medium of titanium, the diffusion processes take place mainly by the interscale mechanism; however, during nitriding, besides the traditional interscale diffusion mechanism, the grain boundary mechanism of diffusion of nitrogen atoms is also realized. The optimal set of surface roughness parameters (height and step parameters, a combination of kurtosis and asymmetry, and profile reference curve parameters) was obtained after boriding. It was determined that the intensity of the adhesive wear of the tribo-pairs with stainless steel and ultrahigh molecular weight polyethylene under dry sliding conditions was influenced not only by the hardness but also roughness of the modified surface layer. The lowest friction coefficient was fixed for the TiB compound layer in both tribo-pairs.

Keywords: titanium Grade 2; surface engineering; nitriding; boriding; surface characteristics; friction

Citation: Lavrys, S.; Pohrelyuk, I.; Tkachuk, O.; Padgurskas, J.; Trush, V.; Proskurnyak, R. Comparison of Friction Behaviour of Titanium Grade 2 after Non-Contact Boriding in Oxygen-Containing Medium with Gas Nitriding. *Coatings* **2023**, *13*, 282. https://doi.org/10.3390/coatings13020282

Academic Editor: Csaba Balázsi

Received: 30 December 2022
Revised: 13 January 2023
Accepted: 23 January 2023
Published: 26 January 2023

1. Introduction

Titanium is well known because of its high specific strength, corrosion resistance, and biocompatibility, which makes it a necessary material for load-bearing biomedical applications (such as hip and knee joints, dental posts, or heart pumps) [1–4]. However, its tribological properties are poor compared to other biomaterials such as Co–Cr alloys and Al_2O_3 ceramics. During friction, there is a local destruction of the native passive oxide film, resulting in the generation of fragments of titanium oxides and local corrosion on the interface. The continuous process of destruction–reconstruction of the oxide film leads to the migration and chemical interaction of fretting wear debris with physiological environment of human body, causing the biological complications (toxicity, carcinogenicity, and inflammation of tissue), and, consequently, implant rejection. Therefore, the wear resistance of titanium is a limiting factor for its use as a bearing material in articulated joint implants. There are many methods for increasing wear and fretting resistance of titanium [5–21], among which diffusion methods (thermochemical treatment) [11–17] are attractive. This is explained by the fact that these methods are technologically simple and provide stable physicochemical and mechanical characteristics of the treated surface. The formed modified surface layers after such treatments have increased hardness, wear resistance, and good adhesion with the base material, etc. Among the large number of diffusion methods, gas nitriding is the most used and attractive one for increasing the functional properties of titanium for medical applications. This method ensures the formation of nitride layers characterized by higher bioinertness, biocompatibility, and wear

and corrosion resistance compared with untreaded titanium and its alloys [14,17,22,23]. For example, the nitride layer formed after gas nitriding provides 4–5 times higher hardness compared with untreated titanium alloy [24]. A better corrosion resistance and a significant decrease in ion release rates for the nitrided alloy (ion release of 1.41 ng/cm^2 compared with 163.58 ng/cm^2 obtained for the commercially pure titanium at pH = 7.48 in artificial Carter–Brugirard saliva) was observed. The cytocompatibility was not compromised and the cell viability performed on human osteoblasts, fibroblastic cells, and epithelial cells was enhanced on the nitrided surface in comparison with the non-nitrided surface. These combined properties make the nitrided Ti-27Nb alloy a good candidate for dental implant applications. Nitriding of Ti-6Al-4V alloy at 850–900 °C improved not only hardness and wear and corrosion resistance but also biocompatibility [25–27]. It was demonstrated that the cell growth and vitality on the nitrided alloy is higher than that on the untreated one [27].

Recently, the attention of scientists has been drawn to diffusion boride layers, which have higher hardness than nitride ones (35 GPa for TiB_2 [28] and 21 GPa for TiB [29] vs. 24 GPa for TiN [30]). Therefore, they allow expected higher wear resistance compared with nitride layers, which indicates the prospect of using boride layers in medical tribocouples. It was also shown in [31] that boride layers on titanium have good cytocompatibility compared with untreated titanium. The good biocompatibility of borides is evidenced by the results [32], where it was shown that TiB_2–Ti composites had a favourable growth rate of cells on their surface within 48 h, as well as excellent compatibility with blood with a low level of haemolysis (<0.12). It was shown that boriding increases corrosion resistance and biocompatibility and decreases the tribocorrosion rate of Ti-6Al-4V alloy [33,34].

However, the main disadvantage of boriding compared with nitriding is the process temperature (for boriding—1100...1500 °C; for nitriding—750...1050 °C) [34,35]. At such high boriding temperatures, the structure of the titanium matrix degrades catastrophically (the rapid growth of grains), which worsens the mechanical and fatigue properties [36–39].

In this research, the prospect of non-contact boriding of titanium in an oxygen-containing medium was considered. Such technology will reduce the temperature of thermodiffusion saturation with boron due to the increasing reactive activity of the boron-containing powder in the abovementioned medium. Because of the presence of an oxygen-containing medium, in addition to a hardened boride layer, a transitional diffusion layer Ti(O) will be formed to avoid a sharp gradient of properties between the boride layer and titanium matrix, and thus this will prevent cracking and detachment of the boride layer. Also, the advantage of this method is the elimination of sticking powder particles to the titanium surface, which improves the quality of the treated surface significantly compared with the traditional solid boriding [39,40].

Therefore, the purpose of this work is to investigate the surface and tribological properties of titanium Grade 2 after non-contact boriding in an oxygen-containing medium and compare them with the properties of titanium after gas nitriding as one of the most well-known and used methods.

2. Materials and Methods

2.1. Investigated Material

The samples of titanium Grade 2 were used. The structure of titanium in the initial state is represented by polyhedral α-grains with a size of 20...40 μm (Figure 1b). The chemical composition and mechanical properties of titanium Grade 2 are given in Table 1 Samples with dimensions of 30 mm × 10 mm × 3 mm were cut from the sheet material by the electroerosion method. The surface of the samples was previously ground and polished to a mirror surface (Figure 1a); the roughness parameter Ra was 0.05 μm.

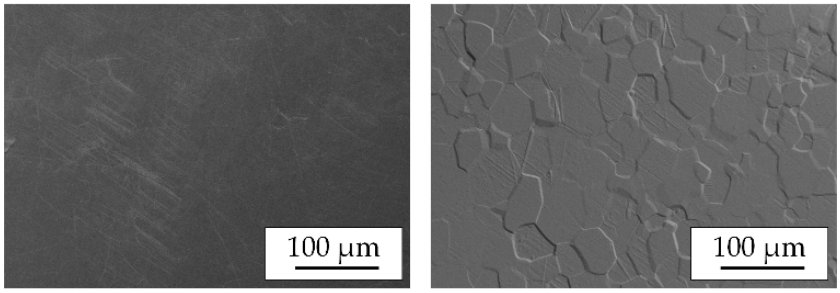

(**a**) (**b**)

Figure 1. Surface topography (**a**) and microstructure (**b**) of titanium Grade 2 in the initial state.

Table 1. Chemical composition and mechanical properties of titanium Grade 2 (according to ISO 5832-2).

Chemical Composition						
Element	N	C	H	Fe	O	Ti
wt. %	0.030	0.100	Maximum 0.015	0.300	0.250	Balance
Mechanical properties						
Hardness, HV						145
Ultimate tensile strength σ, MPa						345
Tensile yield strength $\sigma_{0,2}$, MPa						275
Elongation at break δ, %						20
Reduction of area ψ, %						35
Modulus of elasticity E, GPa						105
Shear modulus G, GPa						110

2.2. Surface Engineering

Thermochemical treatment of titanium was carried out using an equipment developed and manufactured at the Karpenko Physico-Mechanical Institute of the National Academy of Sciences of Ukraine. It allows us to carry out saturation both in a rarefied dynamic atmosphere and in static conditions at atmospheric gas pressure, as well as to reproduce the technological regulation of heat treatment (cyclic changes of temperature and heating and cooling rates) and provides the time–temperature and gas-dynamic regime of saturation in one technological cycle. The methods of gas nitriding [41] and non-contact boriding [38–40] were chosen as the thermochemical treatments of titanium.

Gas nitriding. For gas nitriding, gaseous nitrogen of commercial purity (GOST 9293-74) was used, which before supplying into the reaction chamber of the furnace was dried and freed from oxygen by filtering it through a capsule with silica gel and titanium chips heated up to ~50 °C above the saturation temperature. The titanium samples were placed into the reaction chamber of the furnace in a cylindrical container made of stainless steel and heated in a vacuum to the saturation temperature. The heating rate was 5 °C/min. The reaction gas N_2 was fed into the working chamber after reaching saturation temperature. The nitrogen pressure in the reaction chamber of the furnace was constant (1 atm). After the isothermal holding, the samples were cooled with the furnace (cooling rate ≈ 5 °C/min) in a nitrogen atmosphere to a temperature of 500 °C. Then, the gaseous nitrogen was pumped off and cooling occurred in a vacuum (10^{-3} Pa) (Figure 2a). Based on previous investigations [38,41], the saturation temperatures of 750 °C and 900 °C were chosen because they provide the formation of a layer of compounds consisting only of Ti_2N or a mixture of nitrides (TiN + Ti_2N), respectively.

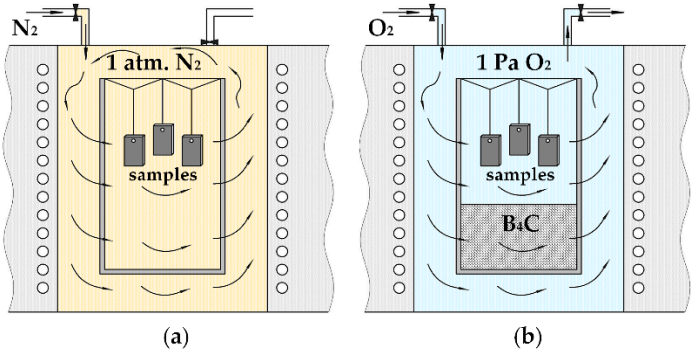

Figure 2. Scheme for fixing of samples during gas nitriding (**a**) and non-contact boriding (**b**).

Non-contact boriding. Boron carbide powder (B_4C) was used as a boron-containing mixture for non-contact boriding. The titanium samples were placed into the reaction chamber of the furnace in a cylindrical container made of stainless steel. A 32 mm-thick layer of boron carbide powder was added into the container. Above the boron-containing powder, the test samples were suspended in a layer at a distance of about 5 mm (Figure 2b). Then, they were heated in a vacuum to the saturation temperature of 900 °C and rarefied oxygen (partial pressure of oxygen ≈ 1 Pa) was added. It circulated both in the furnace chamber and in the container. After the isothermal holding, the samples were cooled with the furnace (cooling rate ≈ 5 °C/min) in rarefied oxygen to a temperature of 500 °C. Then, the oxygen was pumped off and cooling occurred in a vacuum (10^{-3} Pa). It should be noted that the peculiarity of such boriding [38–40] is the presence of an oxygen-containing medium in the furnace atmosphere. In the process of such saturation, the oxygen-containing medium will affect the reaction activity of the components of the medium (backfill). The transport of boron to the surface is realized through the vapour–gas phase, that is, by the reaction of oxygen with boron carbide (oxidation of the powder). As a result, volatile boron suboxide B_2O_2 is formed and it is moved towards the working surface. Then it disproportionates with the formation of boric anhydride B_2O_3 and atomic boron, which diffuses through the interface into titanium and forms the chemical compound TiB on the surface. Under such conditions of boriding, the internal energy of oxygen is sufficient for overcoming the energy barrier, dissolution into titanium, and formation of a solid solution Ti(O) (diffusion layer) [39,42].

2.3. Surface Characterization

The phase composition of the surface layers was determined by X-ray phase analysis using a DRON-3.0 diffractometer in monochromatic CuKα radiation with Bragg–Brentano focusing. The voltage at the anode of the X-ray tube was 30 kV at a current of 25 mA. Diffraction patterns were registered with the help of a step scan in the 2θ angles range 30 . . . 80°. The scan step was 0.05°, and exposure time was 5 s. Sietronix, Powder Cell 2.4 and FullProf software were used to define the locations of diffraction maxima of reflection and identify them according to the JCPDS–ASTM card-file. The analysis of surface topography was carried out using a ZEISS EVO-40XVP scanning electron microscope (SEM) equipped with an INCA Energy 350 energy dispersive X-ray (EDX) microanalysis and backscattered detector (BSD). This allows us to carry out qualitative and quantitative analyses of the content of impurities with an accuracy of 0.01% and automatic scaling and marking of peaks on the spectrum and their reconstruction and comparison. The surface roughness of the samples was investigated via the method of two-step phase-shifting interferometry based on the Twyman–Green interferometer. The microhardness was determined using a PMT-3M durometer under a Vickers indenter with loads of 0.49 and 0.981 N. The nanoindentation was performed using a Micro Combi Tester device with a Vickers diamond indenter. The maximum load during nanoindentation was 200 mN, and the loading and unloading speed was 400 mN/min. The depth of the hardened layer was determined both by the direct method—by changing microstructure of the surface

layers—and by using the microhardness profile across the near-surface layers as the area the microhardness of which exceeds the microhardness of the titanium matrix by 0.2 GPa. The microstructural analysis of the hardened layers and matrix was performed using an Epiquant optical microscope. The sections were etched with Kroll's reagent.

2.4. Friction Testing

The frictional behaviour of titanium after surface engineering was evaluated using the LK-1 friction machine. The friction scheme was «pin-on-plate» during the reciprocating motion. Both 316L stainless steel and ultrahigh molecular weight polyethylene (UHMWPE) were used as the counterbody material. The sliding speed was 0.015 m/s, and the load on the sample was 1 MPa [43–45]. The tests were performed for 1300 cycles with relative displacement stroke between the plate and pin for 30 min. The length of the working stroke of the sample was 20 mm, and the sliding distance was 26 m. The tests were conducted in air (dry sliding). The wear mechanism was evaluated by the worn surface topography.

3. Results and Discussion

3.1. Surface Characteristics

The colour and reflective ability of the titanium surface depended on the method and temperature of the surface treatment. After nitriding at a temperature of 750 °C, the surface is shiny light grey with a golden hue. By increasing temperature to 900 °C, the surface becomes matte with a dark golden hue. The surface of titanium after boriding changes from shiny metallic grey to matte ash-gray (Figure 3). This colour of the surface mainly depends on the titanium nitride or boride, their stoichiometry, thickness, integrity, density, and other characteristics.

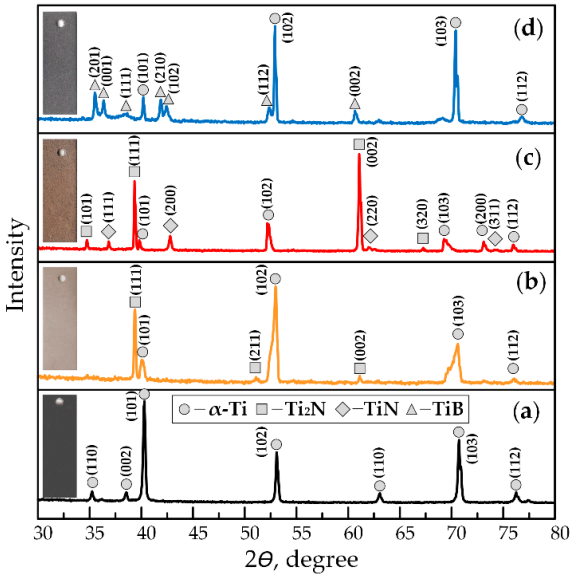

Figure 3. XRD analysis of titanium Grade 2 in the initial state (**a**), after nitriding at temperatures of 750 °C (**b**) and 900 °C (**c**), and after boriding (**d**).

According to the results of the XRD analysis, after nitriding at a temperature of 750 °C, a compound layer of titanium nitride Ti_2N (ε-phase) (77–1893) is formed on the surface of the samples. The (111), (002), and (211) reflections dominate in the diffraction spectrum of Ti_2N. The interplanar distances of α-Ti (44–1294) reflections increase, which indicates the formation of a saturated Ti(N) solid solution under the single-phase nitride layer (Figure 3b). An increase in the nitriding temperature up to 900 °C leads to the formation of a two-phase compound layer that contains both the nitride Ti_2N and the mononitride TiN (δ-phase) (74–1214) (Figure 3c). The (111) and (200) lines dominate in the diffraction spectrum of TiN nitride. The relative intensity of the reflections of the ε-phase of titanium nitride is higher

than the intensity of the reflections of the δ-phase of titanium nitride, which indicates a greater amount of the first phase in the surface layer. The intensity of Ti_2N reflections in the [111] direction increases slightly, but there is a tendency for the appearance of the dominant orientation in the [002] direction, which is evidenced by an increase in the texture coefficient of the (002) plane. It should be noted that by increasing the nitriding temperature, the intensity of the reflections in the nitride phases increases when the intensity of the reflections of α-titanium decreases (Figure 3), which qualitatively indicates the growth and thickening of the nitride film.

After boriding, a wide range of reflections of titanium monoboride TiB (73–2148) of low intensity was fixed in a diffraction spectrum, i.e., a boride layer of compounds was formed (Figure 3d). The intensities of TiB reflections are not high and are fixed in the range of 400–500 relative units, which indicates a negligible content of the latter on the surface. The intensity of α-Ti reflections in the [101] direction decreases, but there is a tendency for an appearance of the dominant orientation in the [102] and [103] directions, as evidenced by an increase of the texture coefficient of the (102) and (103) planes. We also observed a shift in the reflections of the matrix phase (α-titanium) towards the near reflection angles, which indicates greater deformation of the crystal lattice of titanium due to an increase in the amount of interstitial atoms (oxygen). This indirectly indicates the formation of a saturated solid solution of oxygen in titanium Ti(O).

The surface topography of the studied samples in the initial state is mirror-like with individual microscratches. The subsequent nitriding at a temperature of 750 °C slightly changes the surface relief, which indicates uniform penetration of nitrogen atoms into the titanium matrix (Figure 4a). The change in surface relief can be explained by the increased intensity of penetration of the atoms through the grain boundaries, as they are favourable paths for their facilitated diffusion [46–48]. To confirm this hypothesis, an EDX microanalysis of samples after surface treatment was performed, which fixed an increased concentration of nitrogen at the boundaries of titanium grains (Figure 5a and Table 2). This allows assertion that the grain boundaries are new centres of nucleation of nitride films, i.e., on the titanium surface; besides the traditional interscale diffusion mechanism, the grain boundary mechanism of diffusion of nitrogen atoms is also realized. The surface relief increases when the nitriding temperature increases to 900 °C (Figure 4b). The tendency towards greater intensity of penetration of nitrogen atoms through the grain boundaries persists (Figure 5b and Table 2). The surface morphology is complex, resembling a layer-by-layer alternation of nitride layers. It is obvious that by increasing the temperature, the nitride layers grow beyond the grain boundaries, unite, grow one on top of the other, and gradually fill the entire treated surface. As a result, the surface topography repeats the grain boundaries, and this is more pronounced the higher nitriding temperature. It should be noted that according to the results of the EDX microanalysis, the nitrogen content is underestimated, which is explained by the fact that nitrogen has only the N (Kα1) peak (0.392 keV), which unfortunately overlaps with the Ti (Lα1) peak (0.452 keV). Therefore, this analysis does not give a reliable quantitative result regarding the concentration of nitrogen (the content is lower) but allows us to estimate its content qualitatively.

After boriding, the surface topography of the titanium changes. The segregation of spherical TiB monoboride inclusions that cover the entire surface was observed (Figure 4c). A uniform homogeneous layer is formed during boriding, which indicates that under these conditions the diffusion processes take place mainly via the interscale mechanism (Figure 5c). It should also be noted that after boriding from the B_4C powder, only the boride phase of TiB without obvious traces of TiC was fixed. This is explained by the fact that the interaction and formation of titanium carbides during boriding of titanium from B_4C powder is possible at a temperature of 1080 °C [35].

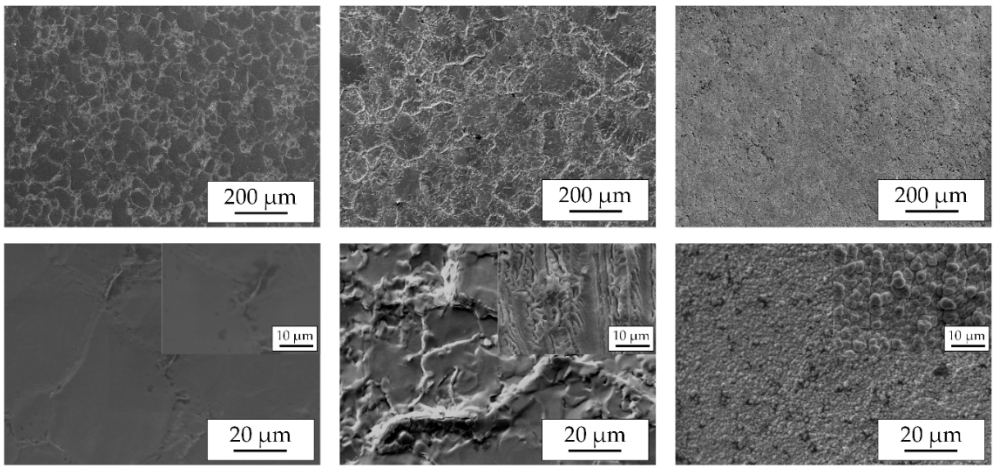

Figure 4. Surface topography of titanium Grade 2 after nitriding at temperatures of 750 °C (**a**) and 900 °C (**b**) and after boriding (**c**).

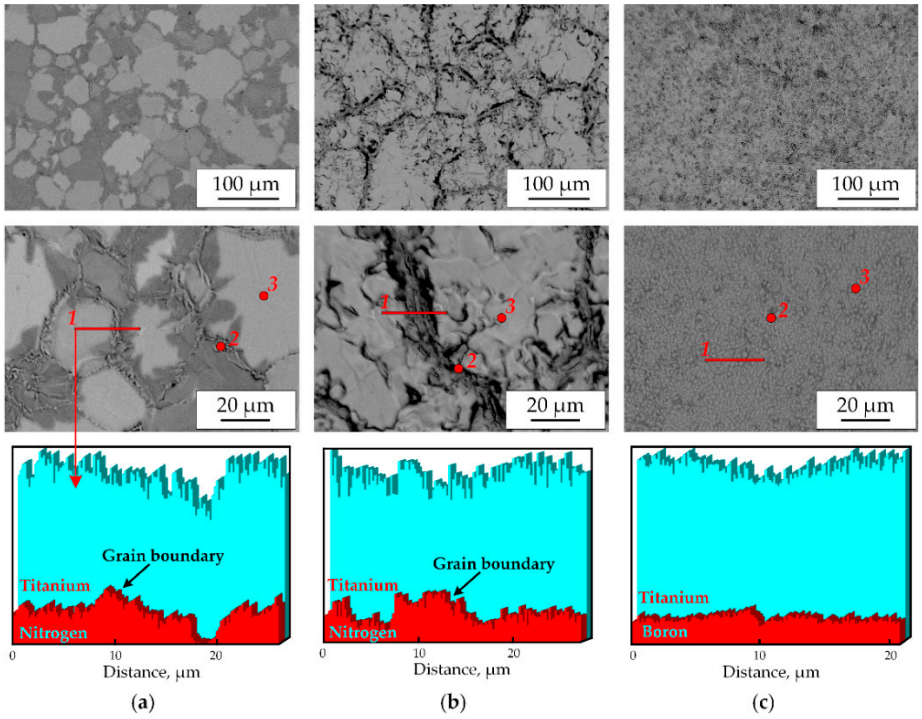

Figure 5. BSD and EDX analysis of titanium Grade 2 surface after nitriding at temperatures of 750 °C (**a**) and 900 °C (**b**) and after boriding (**c**).

Table 2. EDX analysis of titanium Grade 2 surface after surface treatment (see Figure 5).

Surface Treatment	Element	Spectrum №1		Spectrum №2	
		wt., %	at., %	wt., %	at., %
Nitriding at 750 °C	TiK	99.57	89.55	96.29	89.57
	NK	0.43	1.45	3.71	10.43
Nitriding at 900 °C	TiK	91.33	87.13	84.05	80.65
	NK	8.67	12.87	15.95	19.35
Boriding at 900 °C	TiK	58.55	58.22	57.56	54.01
	BK	41.5	41.78	42.44	45.99

The formation of nitride or boride layers on titanium also effects the parameters of surface roughness that were analysed before and after surface treatment using three-dimensional interferograms (Figure 6).

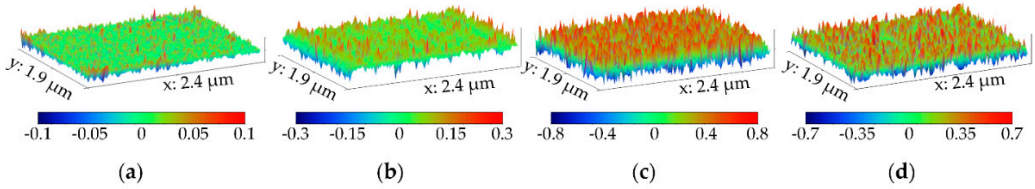

Figure 6. Micro-relief of titanium Grade 2 surface recovered by interferometric method in the initial state (**a**), after nitriding at 750 °C (**b**) and 900 °C (**c**), and after boriding (**d**).

According to the obtained results, it was determined that after nitriding at a temperature of 750 °C, the height parameters of the surface roughness increase by ~2.5...2.7 times and the step parameters decrease slightly (Table 3) due to the fact that a new microrelief is formed on the surface after nitriding where nitride phases of Ti_2N are the new peaks, which are formed at the grain boundaries. By increasing the nitriding temperature to 900 °C, the height parameters increase by 8.5...10.0 times and the step parameters decrease by 2.2...3.3 times (Table 3) due to the formation of the additional peaks of the surface profile because of the formation of the TiN nitride phase.

Table 3. Parameters of surface roughness of titanium Grade 2 after surface treatment.

Surface Treatment	R_a, µm	R_t, µm	R_p, µm	R_v, µm	R_{sk}	R_{ku}	S, µm	S_m, µm	R_{mr}, %
Untreated	0.054	0.241	0.124	0.117	−0.06	2.88	2.21	3.51	0.51
Nitriding at 750 °C	0.134	0.587	0.284	0.303	−0.17	2.89	2.04	3.23	0.47
Nitriding at 900 °C	0.465	1.704	0.741	0.963	−0.042	2.81	1.01	1.06	0.58
Boriding at 900 °C	0.405	1.612	0.854	0.758	−0.04	2.14	1.04	1.44	0.61

After boriding, the height parameters of the surface roughness increase by 6.5...7.5 times and the step parameters decrease by 2.1...2.5 times (Table 3). It should be noted that boriding under the same time–temperature regimen of treatment has a lesser effect on the increase in the height parameters of the surface roughness compared with nitriding. However, both boriding and nitriding reduce the step parameters (Table 3).

The standard height and step characteristics of surface roughness are not always key factors during the prediction of tribological properties of the hardened surface. Therefore, the additional characteristics of surface roughness were determined, namely, the material ratio curve (Abbott–Firestone curve), asymmetry, and kurtosis, which are very important for describing surface relief [49,50].

Nitriding at a temperature of 750 °C leads to a slight decrease in the value of the kurtosis of the surface and reduces the asymmetry parameter by 2.9 times, which characterizes the surface with low peaks and deep valleys (Figure 7). Increasing the temperature of gas nitriding slightly reduces the kurtosis. The coefficient of asymmetry increases and approaches the initial state (untreated) (Figure 7). Such an increase in the asymmetry coefficient occurs due to the growth of the nitride layer, which leads to the formation of a new microrelief and a significant increase in the height parameters of the roughness. The boriding of titanium slightly increases the asymmetry but significantly reduces the kurtosis of the surface (~1.3 times). This is explained by the formation of a new relief with a characteristic surface texture (borides of a spherical shape), which creates low and spreading peaks.

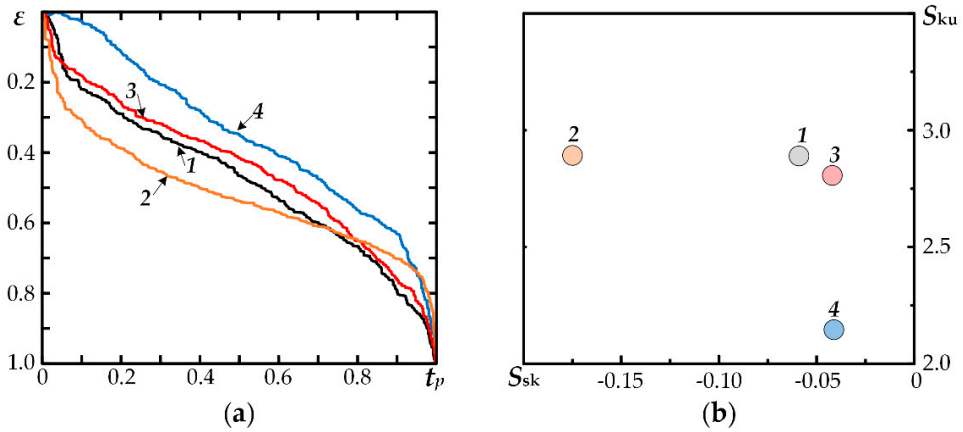

Figure 7. Material ratio curves (**a**) and kurtosis and skewness combination (**b**) of the titanium surface in the initial state (**1**), after nitriding at 750 °C (**2**) and 900 °C (**3**), and after boriding (**4**).

According to the analysis of the material ratio curve (Figure 7b) of the surface, it was established that nitriding at a temperature of 750 °C reduces the value of the material ratio of the profile. However, nitriding and boriding at a temperature of 900 °C increases this value. This is explained by the nucleation and growth of the surface film and the formation of a characteristic relief (Figure 4) that is characterized by low and spreading peaks and deep valleys. It should be noted that the tail part of the material ratio curve rises after all regimes of diffusion treatment, which is evidence of the formation of the wide valleys of the profile. According to studies [38,41], it can be assumed that increasing the material ratio of the profile after nitriding and boriding at a temperature of 900 °C will have a positive effect on the tribological characteristics, especially at runnig-in.

The metallographic analysis established that after surface treatment, near-surface hardened layers are formed on titanium due to the diffusional penetration of the interstitial elements (nitrogen, boron, and oxygen) into the depth of the material. Thus, after nitriding at a temperature of 750 °C, a hardened layer is formed, consisting of a 3 μm-thick nitride Ti_2N layer and a 25 μm-thick diffusion zone. By increasing the nitriding temperature to 900 °C, the hardened layer thickness almost doubles as a result of the intensification of both the processes of nitride formation and gas saturation during nitriding (Figure 8b). Moreover, the morphology of the boride layer differs from nitride one: a continuous layer of compounds is formed during nitriding, and small whiskers of borides TiB with the thickness of 2...5 μm are formed during boriding. They grow deep into the near-surface layer of titanium. Also, as a result of boriding in an oxygen-rich medium, a deep diffusion zone (~80 μm) is formed, consisting of a supersaturated solution of oxygen in titanium Ti(O). It should be noted that at similar temperatures, boriding in an oxygen-containing medium provides a deeper diffusion layer than nitriding due to the higher diffusion coefficient of oxygen against nitrogen in titanium and, as a result, the higher intensity of gas saturation [39].

Considering the fact that nitriding or boriding is carried out at high temperatures, this affects the microstructure of the titanium matrix. Thus, nitriding at a temperature of 750 °C increases the size of titanium grains by ~4 times, which is associated with the processes of recrystallization of the alloy. Increasing the temperature to 900 °C intensifies the processes of recrystallization and leads to an increase in the size of the grains. It should also be noted that at temperatures close to β-transus, the processes of recrystallization of some α-grains with the formation of secondary acicular α-grains against the background of the primary ones also occur (Figure 9).

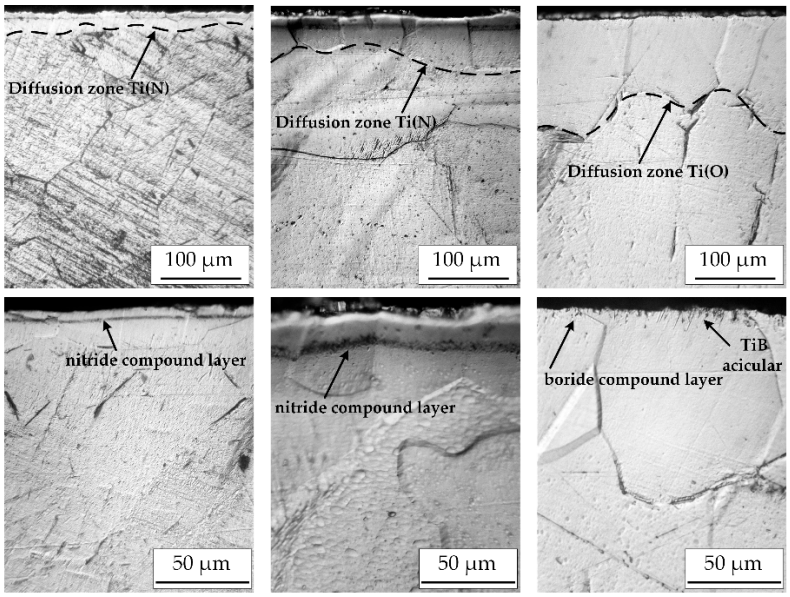

Figure 8. Microstructure of the near-surface layer of titanium Grade 2 after nitriding at 750 °C (**a**) and 900 °C (**b**) and after boriding (**c**).

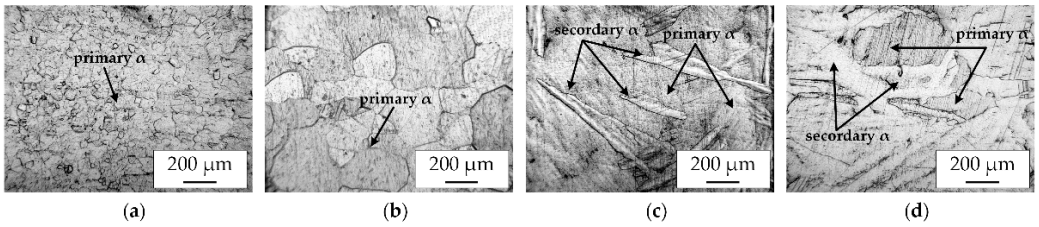

Figure 9. Microstructure of near-surface layer of titanium Grade 2 in initial state (**a**) and after nitriding at 750 °C (**b**) and 900 °C (**c**) and after boriding (**d**).

Furthermore, the formation of nitride or boride layers effects the level of the surface hardening of titanium. The surface microhardness of titanium increases by 2.5 times after nitriding at a temperature of 750 °C (Table 4). Nitriding at a temperature of 900 °C increases the microhardness by almost 8 times compared with the initial state due to the activation of phase formation processes and the formation of TiN mononitride. The formation of a TiB boride layer on the surface provides higher microhardness than a Ti_2N layer but does not exceed the hardness of a TiN + Ti_2N layer.

Based on the results of nanoindentation, it was established that the relationship between surface treatment and hardness is preserved. With an increase in the nanohardness and the Young's modulus, the resistance to elastic deformation of the surface layer increases. Young's modulus characterizes the ability of samples to resist elastic deformation. When Young's modulus was large, the amount of elastic recovery was large during the unit time. As shown in Figure 10, the sample has better resistance to deformation after nitriding at 900 °C. This phenomenon can be interpreted by the fundamental theory of indentation based on the Oliver–Pharr method. It was shown in [51] that residual tensile stress will increase the indent depth and shift the load-depth curve toward the right, which results in lower hardness. Also during indentation of untreated titanium, a sudden displacement burst at shallow indentation depths was observed. This appeared as a plateau in the loading curve (so-called pop-in) (Figure 10a) due to the destruction of a thin passive film on the titanium (Figure 11a). It should be noted that for nitride layers we observed a rather high scatter for the nanoindentation data, which can be explained as follows: the intensity of nitride formation is higher at the grain boundaries than in the grain body (Figure 5);

therefore, there is a deeper nitride layer and, as a result, higher hardness (Figures 10 and 11). This effect was not observed for borided titanium, which indicates the homogeneity of the surface layer.

Table 4. Results of durometric analysis of titanium Grade 2 after surface treatment.

Surface Treatment	Microindentation		Nanoindentation				Deep of Layer, μm
	$HV_{0.98}$, ГПа	$HV_{0.49}$, ГПа	H_{IT}, ГПа	E_{IT}, ГПа	C_{IT}, %	η_{IT}	
Untreated	1.47	1.51	2.66	134.7	2.48	12.8	–
Nitriding at 750 °C	3.56	3.84	11.47	191.3	1.25	38.2	26
Nitriding at 900 °C	12.23	14.46	16.29	238.9	0.48	50.2	49
Boriding at 900 °C	8.91	9.12	13.37	191.6	0.41	38.4	86

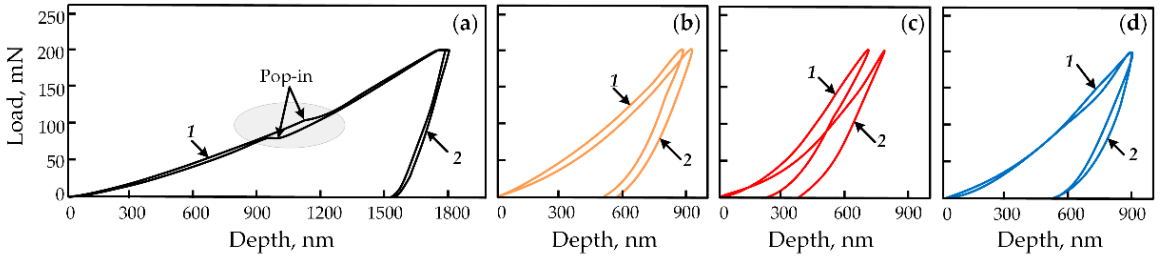

Figure 10. Loading and unloading curves of titanium Grade 2 during nanoindentation in initial state (**a**) and after nitriding at 750 °C (**b**) and 900 °C (**c**) and after boriding (**d**): 1 and 2—nanoindentation near grain boundary and in grain body, respectively.

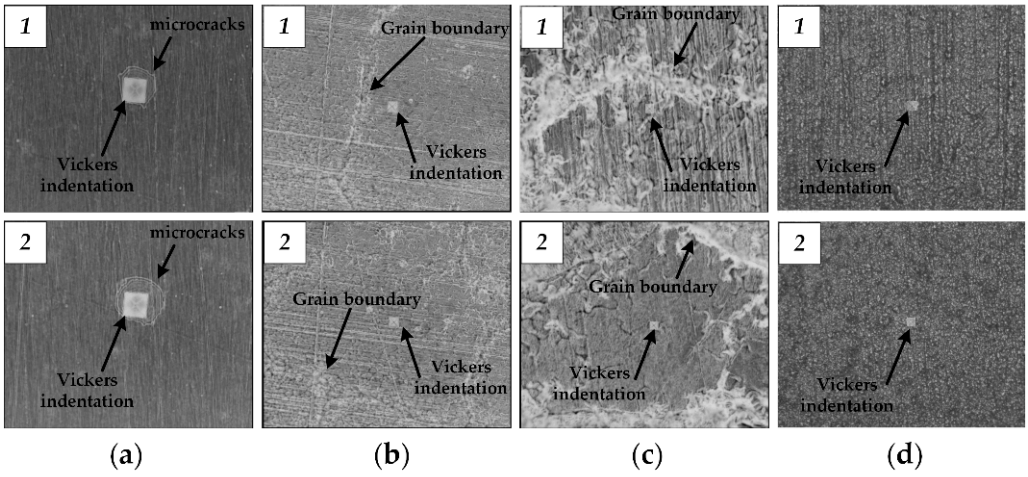

Figure 11. Imprint of Vickers pyramid on surface of titanium Grade 2 in initial state (**a**), after nitriding at 750 °C (**b**) and 900 °C (**c**), and after boriding (**d**): 1 and 2—nanoindentation near grain boundary and in grain body, respectively.

The results of the microhardness distribution (Figure 12) in the near-surface layer agree well with the metallographic analysis. Boriding in an oxygen-containing medium provides the deepest layer and a smoother gradient with a higher level of hardening.

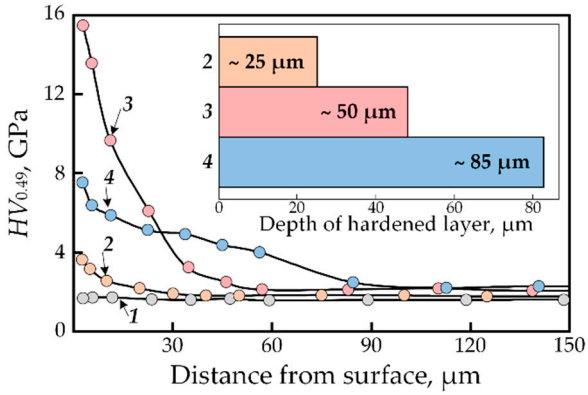

Figure 12. Hardness distribution in the surface layer of titanium Grade 2 in initial state (1), after nitriding (2, 3), and after boriding (4).

3.2. Friction Behaviour

3.2.1. Friction Behaviour of Surface Hardened Titanium Grade 2 in a Tribo-Pair with Stainless Steel

According to the results of the tribological tests, it was established that the worst antifriction properties (the highest friction coefficient) are fixed for untreated titanium (Figure 13a). This is explained by the fact that during the friction of untreated titanium in the tribo-pair with steel, an adhesive wear mechanism is realized. That is, due to the high chemical activity and low thermal conductivity of titanium, processes of microwelding and tearing of titanium from the surface occur during friction. As a result, we fix the adhesive craters on the contact surface of the samples with lower hardness (titanium), which later stick to the surface of harder material (steel) (Figure 14a).

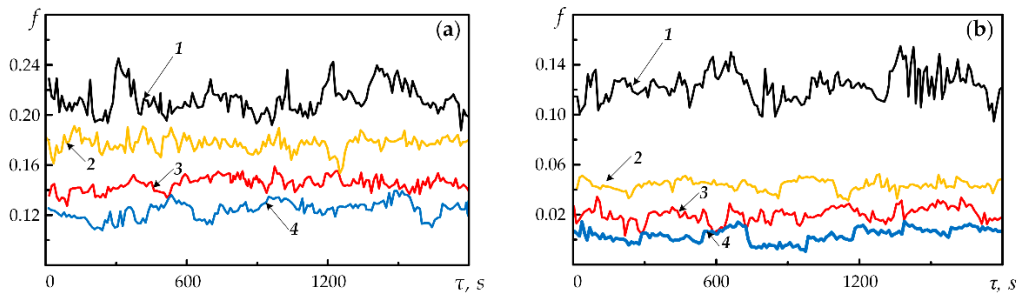

Figure 13. Friction coefficient of titanium Grade 2 in tribo-pairs with 316L stainless steel (**a**) and UHMWPE (**b**): in initial state (1), after nitriding at 750 °C (2) and 900 °C (3), and after boriding (4).

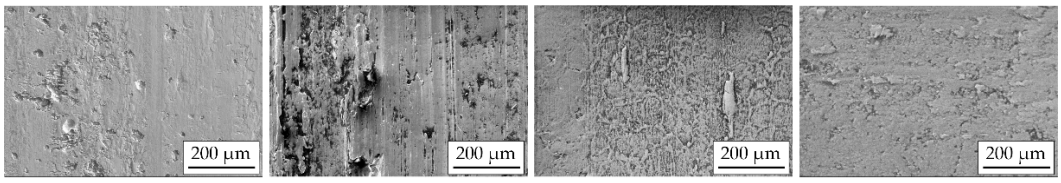

Figure 14. SEM images of wear tracks after friction with 316L stainless steel; untreated titanium (**a**), nitrided samples at 750 °C (**b**) and 900 °C (**c**), and borided sample (**d**).

The thermochemical treatment (nitriding and boriding) improves the antifriction properties of titanium (Figure 13a). It is associated with the formation of chemically inert and hard nitride and boride layers, which change the nature of adhesive wear: steel wears more intensively. This is confirmed by the metallographic analysis of the wear surfaces: the sticking of the counterbody material (steel) on the surface of the treated titanium was fixed (Figure 14b–d).

It should be noted that nitriding at a temperature of 750 °C improves the antifriction properties of titanium the least (Figure 13a). It is obvious that under such friction conditions the thin nitride (compound) layer on the titanium surface is destroyed easily due to the high specific load at the contact points, which leads to the baring of the chemically clean surface. As a result, the partial seizure and tearing of titanium along the grain boundaries occurred. Thus, according to the SEM analysis, the Ti_2N wear surface is characterized by deep grooves along the grain boundaries where the material is pulled out (Figure 14b).

The highest antifriction properties for titanium are provided by nitriding and boriding at a temperature of 900 °C. Thus, according to the metallographic analysis, a decrease in the adhesive and an increase in the abrasive component of wear is observed on the topography of TiN and TiB wear surfaces. It obviously improves the frictional behaviour of titanium. It should be noted that the better antifriction characteristics of titanium are fixed after boriding of titanium, which is obviously related to the higher surface quality (lower roughness parameter Ra) of the TiB surface than the TiN surface (Figure 4).

3.2.2. Friction Behaviour of Surface Hardened Titanium Grade 2 in a Tribo-Pair with UHMWPE

In the tribo-pairs with UHMWPE, the lowest antifriction properties of titanium are fixed in the initial state (untreated) (Figure 13b). The wear mechanism of this tribo-pair is adhesive where we fixed the transfer of UHMWPE to the titanium surface (Figure 15a). It should be noted that we fixed burrs on the surface, which are located perpendicular to the direction of friction. It is obvious that such burrs promote the destruction of the natural oxide film, which will worsen the frictional behaviour of titanium.

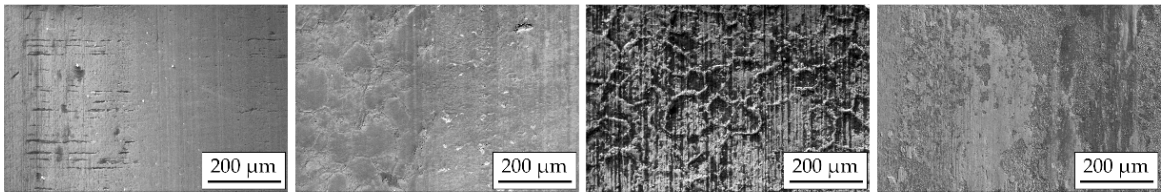

Figure 15. SEM images of wear tracks after friction with UHMWPE; untreated titanium (**a**), nitrided samples at 750 °C (**b**) and 900 °C (**c**), and borided sample (**d**).

The thermochemical treatment improves the antifriction properties of titanium in a tribo-pair with UHMWPE. However, in contrast to the tribo-pair with steel, the main characteristics that affect the frictional behaviour of titanium to a greater extent are the surface quality, roughness, and morphology of the layer and to a lesser extent, the hardness. Thus, nitriding at 750 °C provides less surface roughness and relief, which contributes to better antifriction properties for titanium than nitriding at 900 °C. This is explained by the fact that during nitriding, a characteristic nitride layer is formed, which reproduces the boundaries of titanium grains. Thus, during friction, the relief nitride film, like an abrasive, will plow through the soft material of the counterbody, i.e., the adhesive wear will intensify the processes of abrasive wear. By increasing nitriding temperature, the surface roughness increases and worsens the wear and frictional behaviour of the tribo-pair. Boriding, due to the formation of a homogeneous boride layer with low roughness, improves the frictional behaviour of titanium in a tribo-pair with UHMWPE compared with nitriding.

4. Conclusions

In this work, the comparison of the friction behaviour of titanium Grade 2 after non-contact boriding in oxygen-containing medium with gas nitriding was studied. The main conclusions are as follows:

1. It was determined that the single-phase (Ti_2N) or two-phase (Ti_2N + TiN) compound layers were formed during the nitriding of titanium at temperatures of 750 °C or

900 °C. The single-phase (TiB) compound layer was formed after non-contact boriding in oxygen-containing medium.

2. It was shown that non-contact boriding allows formation of a homogeneous compound layer with better surface roughness (height, step, and other parameters) compared with gas nitriding. According to the results of micro- and nanoindentation tests, boriding provides a deeper hardened layer but lower surface hardness and elastic modulus.
3. It was found that borided titanium has better friction behaviour under dry sliding in tribo-pairs with stainless steel (friction coefficient is lower by ~1.5 times) and UHMWPE (friction coefficient is lower by ~2 times) in comparison with nitriding.
4. According to the SEM analysis, it was determined that formation of the compound layers on titanium leads to a decrease in the adhesive component and an increase in the abrasive one of the wear mechanism in tribo-pairs. Boriding, due to better roughness, provides the decrease in adhesive and abrasive wear compared with nitriding.

Author Contributions: S.L.: conceptualization, mechanism research, investigation, writing-original draft and SEM and EDX investigations; I.P.: conceptualization, supervision, project management, writing-review and editing; O.T: writing—original draft preparation and XRD investigation; J.P.: nanoidentation and friction test; V.T: formal analysis and methodology; R.P.: metallographic analysis. All authors have read and agreed to the published version of the manuscript.

Funding: This research received no external funding.

Institutional Review Board Statement: Not applicable.

Informed Consent Statement: Not applicable.

Data Availability Statement: The data presented in this study are available upon request from the corresponding author.

Conflicts of Interest: The authors declare no conflict of interest.

References

1. Hernández-López, J.M.; Conde, A.; de Damborenea, J.J.; Arenas, M.A. Electrochemical response of TiO_2 anodic layers fabricated on Ti6Al4V alloy with nanoporous, dual and nanotubular morphology. *Corros. Sci.* **2016**, *112*, 194–203. [CrossRef]
2. Xiu, P.; Jia, Z.; Li, J.; Yin, C.; Cai, H.; Song, C.; Cheng, Y. Hierarchical micropore/nanorod apatite hybrids in-situ grown from 3-D printed macroporous Ti6Al4V implants with improved bioactivity and osseointegration. *J. Mater. Sci. Technol.* **2017**, *33*, 179–186. [CrossRef]
3. Xin, Z.; Ren, N.; Ren, Y.; Yue, X.; Han, Q.; Zhou, W.; Tao, Y.; Ye, Y. In-situ nitriding on the textured titanium alloy using femtosecond laser. *J. Mater. Res. Technol.* **2022**, *19*, 466–471. [CrossRef]
4. Subramanian, B.; Muraleedharan, C.V.; Ananthakumar, R.; Jayachandran, M. A comparative study of titanium nitride (TiN), titanium oxy nitride (TiON) and titanium aluminum nitride (TiAlN), as surface coatings for bio implants. *Surf. Coat. Technol.* **2011**, *205*, 5014–5020. [CrossRef]
5. Wang, S.; Liu, Y.; Zhang, C.; Liao, Z.; Liu, W. The improvement of wettability, biotribological behavior and corrosion resistance of titanium alloy pretreated by thermal oxidation. *Tribol. Int.* **2014**, *79*, 174–182. [CrossRef]
6. Nykyforchyn, H.M.; Agarwala, V.S.; Klapkiv, M.D.; Posuvailo, V.M. Simultaneous reduction of wear and corrosion of titanium, magnesium and zirconium alloys by surface plasma electrolytic oxidation treatment. *Adv. Mater. Res.* **2008**, *38*, 27–35. [CrossRef]
7. Hutsaylyuk, V.; Student, M.; Posuvailo, V.; Student, O.; Hvozdets'kyi, V.; Maruschak, P.; Zakiev, V. The role of hydrogen in the formation of oxide-ceramic layers on aluminum alloys during their plasma-electrolytic oxidation. *J. Mater. Res. Technol.* **2021**, *14*, 1682–1696. [CrossRef]
8. Błoniarz, A.; Cholewa-Kowalska, K.; Gajewska, M.; Grysakowski, B.; Moskalewicz, T. Electrophoretic deposition, microstructure and selected properties of nanocrystalline SnO2/Sr enriched bioactive glass/chitosan composite coatings on titanium. *Surf. Coat. Technol.* **2022**, *450*, 129004. [CrossRef]
9. Bajda, S.; Liu, Y.; Tosi, R.; Cholewa-Kowalska, K.; Krzyzanowski, M.; Dziadek, M.; Kopyscianski, M.; Dymek, S.; Polyakov, A.V.; Semenova, I.P.; et al. Laser cladding of bioactive glass coating on pure titanium substrate with highly refined grain structure. *J. Mech. Behav. Biomed. Mater.* **2021**, *119*, 104519.
10. Liu, S.; Xia, C.; Liu, Z.; Ma, J.; Hu, Y.; Wang, H.; Liang, C.; Yang, L.; Zhou, H. Micro-arc oxidation preparation of a ZnO-Se composite coating on titanium with anti-oxidation and anti-bacterial potentials for osteomyelitis control. *Mater. Lett.* **2022**, *327*, 132979. [CrossRef]

11. Nakai, M.; Niinomi, M.; Akahori, T.; Ohtsu, N.; Nishimura, H.; Toda, H.; Fukui, H.; Ogawa, M. Surface hardening of biomedical Ti–29Nb–13Ta–4.6Zr and Ti–6Al–4V ELI by gas nitriding. *Mater. Sci. Eng. A* **2008**, *486*, 193–201. [CrossRef]
12. Pohrelyuk, I.; Tkachuk, O.; Proskurnyak, R.; Guspiel, J.; Beltowska-Lehman, E.; Morgiel, J. Influence of regulated modification of nitride layer by oxygen on electrochemical behavior of Ti–6Al–4V alloy in Ringer's solution. *Mater. Corros.* **2019**, *70*, 2320–2325. [CrossRef]
13. Pohrelyuk, I.M.; Padgurskas, J.; Tkachuk, O.V.; Luk'yanenko, A.G.; Trush, V.S.; Lavrys, S.M. Influence of oxynitriding on antifriction properties of Ti–6Al–4V titanium alloy. *J. Frict. Wear* **2020**, *41*, 333–337. [CrossRef]
14. Pohrelyuk, I.M.; Sheykin, S.E.; Dub, S.M.; Mamalis, A.G.; Rostotskii, I.Y.; Tkachuk, O.V.; Lavrys, S.M. Increasing of functionality of c.p. titanium/UHMWPE tribo-pairs by thermodiffusion nitriding of titanium component. *Biotribology* **2016**, *7*, 38–45. [CrossRef]
15. Manhabosco, T.M.; Tamborim, S.M.; dos Santos, C.B.; Müller, I.L. Tribological, electrochemical and tribo-electrochemical characterization of bare and nitrided Ti6Al4V in simulated body fluid solution. *Corros. Sci.* **2011**, *53*, 1786–1793. [CrossRef]
16. Anusha Thampi, V.V.; Chukwuike, V.I.; Shtansky, D.V.; Subramanian, B. Biocompatibility study of nanocomposite titanium boron nitride (TiBN) thin films for orthopedic implant applications. *Surf. Coat. Technol.* **2021**, *410*, 126968.
17. Rahmatian, B.; Ghasemi, H.M.; Heydarzadeh Sohi, M.; de Baets, P. Tribocorrosion and corrosion behavior of double borided layers formed on Ti-6Al-4V alloy: An approach for applications to bio-implants. *Corros. Sci.* **2023**, *210*, 110824. [CrossRef]
18. Paleu, C.C.; Munteanu, C.; Istrate, B.; Bhaumik, S.; Vizureanu, P.; Bal, M.S.; Paleu, V. Microstructural analysis and tribological behavior of amdry 1371 (mo–nicrfebsic) atmospheric plasma spray deposited thin coatings. *Coatings* **2020**, *10*, 1186. [CrossRef]
19. Baltatu, M.S.; Vizureanu, P.; Sandu, A.V.; Munteanu, C.; Istrate, B. Microstructural analysis and tribological behavior of Ti-based alloys with a ceramic layer using the thermal spray method. *Coatings* **2020**, *10*, 1216. [CrossRef]
20. Cura, A.C.; Zuchua, J.I.; Tribbia, L.T.; Taravini, I.R.; Decco, E.O.A. Sandblasted, acid etched and UV irradiated titanium surface for dental implants: In vitro and in vivo analysis. *Materialia* **2022**, *21*, 101302. [CrossRef]
21. Özmeriç, N.; Çakal, G.Ö.; Gökmenoğlu, C.; Özmeriç, A.; Oduncuoğlu, B.F.; Hacaloğlu, T.; Kaftanoğlu, B. Histomorphometric and biomechanical evaluation of the osseointegration around micro- and nano-level boron-nitride coated titanium dental implants. *J. Stomatol. Oral Maxillofac. Surg.* **2022**, *123*, 694–700. [CrossRef] [PubMed]
22. Zhao, G.-H.; Aune, R.E.; Espallargas, N. Tribocorrosion studies of metallic biomaterials: The effect of plasma nitriding and DLC surface modifications. *J. Mech. Behav. Biomed. Mater.* **2016**, *63*, 100–114. [CrossRef] [PubMed]
23. Venkatesan, S.P.; Jeevahan, J.; Purusothaman, M.; Venkatesh, S.; Rakesh Vimal, M. Corrosion and mechanical behavior of plasma nitrated metallic biomaterial surfaces. *Mater. Today: Proc.* **2021**, *47*, 938–943. [CrossRef]
24. Bédouin, Y.; Gordin, D.-M.; Pellen-Mussi, P.; Pérez, F.; Tricot-Doleux, S.; Vasilescu, C.; Drob, S.I.; Chauvel-Lebret, D.; Gloriant, T. Enhancement of the biocompatibility by surface nitriding of a low-modulus titanium alloy for dental implant applications. *J. Biomed. Mater. Res. B Part B* **2019**, *107*, 1483–1490. [CrossRef]
25. Jambagi, S.C.; Malik, V.R. A review on surface engineering perspective of metallic implants for orthopaedic applications. *JOM* **2021**, *73*, 4349–4364. [CrossRef]
26. Tamura, Y.; Yokoyama, A.; Watari, F.; Kawasaki, T. Surface properties and biocompatibility of nitrided titanium for abrasion resistant implant materials. *Dent. Mater. J.* **2002**, *21*, 355–372. [CrossRef] [PubMed]
27. Pohrelyuk, I.M.; Tkachuk, O.V.; Proskurnyak, R.V.; Boiko, N.M.; Kluchivska, O.Y.; Stoika, R.S. Effect of thermodiffusion nitriding on cytocompatibility of Ti-6Al-4V titanium alloy. *JOM* **2016**, *68*, 1109–1115. [CrossRef]
28. Sun, L.; Gao, Y.; Xiao, B.; Li, Y.; Wang, G. Anisotropic elastic and thermal properties of titanium borides by first-principles calculations. *J. Alloys Compd.* **2013**, *579*, 457–467. [CrossRef]
29. Sivakumar, B.; Pathak, L.C.; Singh, R. Fretting corrosion response of boride coated titanium in Ringer's solution for bio-implant use: Elucidation of degradation mechanism. *Tribol. Int.* **2018**, *127*, 219–230. [CrossRef]
30. Siyuan, W.U.; Shoujun, W.U.; Guoyun, Z.; Weiguo, Z. Hardness and elastic modulus of titanium nitride coatings prepared by pirac method. *Surf. Rev. Lett.* **2018**, *25*, 1850040.
31. Miklaszewski, A.; Jurczyk, M.U.; Jurczyk, K.; Jurczyk, M. Plasma surface modification of titanium by TiB precipitation for biomedical applications. *Surf. Coat. Technol.* **2011**, *206*, 330–337. [CrossRef]
32. Makau, F.M.; Morsi, K.; Gude, N.; Alvarez, R.; Sussman, M.; May-Newman, K. Viability of titanium-titanium boride composite as a biomaterial. *ISRN Biomater.* **2013**, *2013*, 970535. [CrossRef]
33. Sivakumar, B.; Singh Lokesh, R.; Pathak, C.L. Corrosion behavior of titanium boride composite coating fabricated on commercially pure titanium in Ringer's solution for bioimplant applications. *Mater. Sci. Eng. C* **2015**, *48*, 243–255. [CrossRef] [PubMed]
34. Sivakumar, B.; Pathak, L.C.; Singh, R. Response of boride coating on the Ti-6Al-4V alloy to corrosion and fretting corrosion behavior in Ringer's solution for bio-implant application. *Appl. Surf. Sci.* **2018**, *433*, 1158–1174.
35. Duan, Y.; Wang, X.; Liu, D.; Bao, W.; Li, P.; Peng, M. Characteristics, wear and corrosion properties of borided pure titanium by pack boriding near $\alpha \rightarrow \beta$ phase transition temperature. *Ceram. Int.* **2020**, *46*, 16380–16387. [CrossRef]
36. Zhang, H.; Zhang, F.; Fu, L.; Wan, Q. Spark plasma sintering assisted rapid growth of titanium boride layers on titanium: Microstructures and growth kinetics. *Surf. Coat. Technol.* **2022**, *432*, 128083. [CrossRef]
37. Aich, S.; Ravi, K.; Chandran, S. TiB whisker coating on titanium surfaces by solid-state diffusion: Synthesis, microstructure, and mechanical properties. *Metall. Mater. Trans. A* **2002**, *33*, 3489–3498. [CrossRef]
38. Pohrelyuk, I.M.; Lavrys, S.M.; Stasyshyn, I.V.; Penkovyi, O.V. Influence of thermochemical treatment on the surface topography of titanium. *Metallofiz. Noveishie Tekhnol.* **2017**, *39*, 1183–1196. [CrossRef]

39. Prytula, A.O.; Pogrelyuk, I.N.; Fedirko, V.N. Effect of impregnating atmosphere oxygen on boriding of titanium alloys. *Met. Sci. Heat Treat.* **2008**, *50*, 232–237. [CrossRef]
40. Pohrelyuk, I.M.; Vasyliv, K.B.; Fedirko, V.M.; Sambors'kyi, O.V. Structure and topography of the surfaces of titanium alloys after thermodiffusion saturation from boron carbide in vacuum. *Mater. Sci.* **2010**, *46*, 348–356. [CrossRef]
41. Pohrelyuk, I.M.; Lavrys, S.M.; Sakharuk, O.M.; Stasyshyn, I.V.; Penkovyi, O.V. Pretreatment influence on titanium surface properties after gas nitriding. *J. Mater. Eng. Perform.* **2017**, *26*, 5072–5078. [CrossRef]
42. Kaplan, Y.; Cetin Can, A.; Ulukoy, A. A new medium for boriding of Ti6Al4V alloy for biomedical applications. *Proc. Inst. Mech. Eng. Part L J. Mater. Des. Appl.* **2019**, *233*, 109–111. [CrossRef]
43. Gispert, M.P.; Serro, A.P.; Colaço, R.; Botelho do Rego, A.M.; Alves, E.; da Silva, R.C.; Brogueira, P.; Pires, E.; Saramago, B. Tribological behaviour of Cl-implanted TiN coatings for biomedical applications. *Wear* **2007**, *262*, 1337–1345. [CrossRef]
44. Xiong, D.; Gao, Z.; Jin, Z. Friction and wear properties of UHMWPE against ion implanted titanium alloy. *Surf. Coat. Technol.* **2007**, *201*, 6847–6850. [CrossRef]
45. Kusy, R.P.; Tobin, E.J.; Whitley, J.Q.; Sioshansi, P. Frictional coefficients of ion-implanted alumina against ion-implanted beta-titanium in the low load, low velocity, single pass regime. *Dent. Mater.* **1992**, *8*, 167–172. [CrossRef] [PubMed]
46. Ge, L.; Tian, N.; Lu, Z.; You, C. Influence of the surface nanocrystallization on the gas nitriding of Ti–6Al–4V alloy. *Appl. Surf. Sci.* **2013**, *286*, 412–416. [CrossRef]
47. Farokhzadeh, K.; Qian, J.; Edrisy, A. Effect of SPD surface layer on plasma nitriding of Ti–6Al–4V alloy. *Mater. Sci. Eng. A* **2014**, *589*, 199–208. [CrossRef]
48. Takesue, S.; Kikuchi, S.; Akebono, H.; Misaka, Y.; Komotori, J. Effect of pre-treatment with fine particle peening on surface properties and wear resistance of gas blow induction heating nitrided titanium alloy. *Surf. Coat. Technol.* **2019**, *359*, 476–484. [CrossRef]
49. Chen, H.; Xu, C.; Xiao, G.; Yi, M.; Chen, Z.; Zhang, J. Analysis of the relationship between roughness parameters of wear surface and tribology performance of 5CB liquid crystal. *J. Mol. Liq.* **2022**, *352*, 118711. [CrossRef]
50. Sedlaček, M.; Podgornik, B.; Vižintin, J. Correlation between standard roughness parameters skewness and kurtosis and tribological behaviour of contact surfaces. *Tribol. Int.* **2012**, *48*, 102–112. [CrossRef]
51. Chen, T.; Koyama, S. Influence of boriding temperature on microstructure and tribological properties of titanium. *Solid State Sci.* **2020**, *107*, 106369. [CrossRef]